Sensors & Diagnostics

Accepted Manuscript

This article can be cited before page numbers have been issued, to do this please use: S. Singh, S. K. Dubey and S. Goel, *Sens. Diagn.*, 2026, DOI: 10.1039/D6SD00005C.

ROYAL SOCIETY OF CHEMISTRY

rsc.li/sensors

DOI: 10.1039/D6SD00005C

Highly Sensitive Electrochemical Sensor for Uric Acid Using Additively Manufactured Miniaturized Microelectrodes for Point of Care Application

Sanjeet Kumar[1,3], Satish Kumar Dubey[1,3] and Sanket Goel[1,2]

[1]*MEMS, Microfluidics and Nanoelectronics (MMNE) Lab, Birla Institute of Technology and Science (BITS) Pilani, Hyderabad Campus, Hyderabad 500078, India*

[2]*Department of Electrical and Electronics Engineering, Birla Institute of Technology and Science (BITS) Pilani, Hyderabad Campus, Hyderabad 500078, India*

[3]*Department of Mechanical Engineering, Birla Institute of Technology and Science (BITS) Pilani, Hyderabad Campus, Hyderabad 500078, India*

**Corresponding Author's Email Address: sgoel@hyderabad.bits-pilani.ac.in , satishdubey@hyderabad.bits-pilani.ac.in*

Abstract

Point of care (PoC) biofluid diagnostics is hindered by the fundamental limitations of traditional electrochemical platforms, namely their complex fabrication, prohibitive cost, and reliance on benchtop instruments. To address these challenges, a simple additive manufacturing based sensor fabrication strategy was employed to develop a miniaturized platform to make it compatible with portable electrochemical devices, creating an advanced diagnostic system capable of detecting the hyperuricemia biomarker in serum samples. In this work, a rapid and ultrasensitive diagnostic device utilizing a 3D printed carbon conductive electrode with a carboxylic group mediated enzymatic platform was developed to detect uric acid. This study introduces a highly sensitive 3D printed microelectrode integrated with a wireless potentiostat for the rapid detection of uric acid (UA). The developed portable platform exhibits excellent analytical performance in the concentration range of 10–500 μM, with an ultralow detection limit of 7.95 μM achieved by chronoamperometry (CA) techniques. The device demonstrates improved selectivity, high sensitivity, and 28-day stability without interference. The real sample study was carried out using CA in serum sample and the recovery percentage found as 97%. The results also illustrate seamless integration with miniaturized electrochemical platform acquired from a portable potentiostat detection system, and user-friendly operation. Overall, this platform enables scalable and customizable fabrication of miniaturized biosensors, paving the way for decentralized clinical

View Article Online
DOI: 10.1039/D6SD00005C

diagnostics, point of care testing, wearable health monitoring, and field deployable biosensing applications.

Keywords: Additive manufacturing; Miniaturized Biosensor; Point of care detection; Uric acid; Electrochemical; Hyperuricemia; Chronic Kidney Disease

1. Introduction

Uric acid (UA) is a key clinical biomarker for the detection of gout, hyperuricemia, and chronic kidney disease. It is the final product of purine nucleotide metabolism, primarily excreted by the kidneys [1][2]. The clinical range of the UA, concentration range in the healthy body typically ranges from 130 to 460 µmol (3.5–7.2 mg/dL) in males, and in females from 240 to 510 µmol/L (2.7-7.3 mg/dL). These ranges can vary depending on factors such as diet, age, gender, and genetics [3]. Abnormal UA levels indicate several associated pathological conditions. Hyperuricemia, defined as UA levels exceeding 420 µmol/L in males and 360 µmol/L in females, is a significant risk factor that can lead to gout, kidney stones, hypertension, cardiovascular disease, chronic kidney disease, and metabolic syndrome [4][1][2][5]. Hypouricemia is very rare, but it may indicate an underlying metabolic or genetic disorder such as Wilson's disease or Fanconi syndrome [6]. This critical clinical measure enables accurate and timely disease detection in patients, facilitating prognosis, diagnosis, management, and therapeutic monitoring [3]. Additive manufacturing, also known as three dimensional printing (3D), has emerged as a critical fabrication technology for the development of biosensors and other diagnostic devices[7] [8,9][10][11]. The potential of these materials is driving research into biosensors by its excellent mechanical strength and necessary electrical conductivity, promising the creation of low-cost, portable platforms for point-of-care testing (POCT)[12]. A few groups have successfully implemented this technology for the detection of clinical biomarkers such as hydrogen peroxide (H_2O_2), glucose (Glu), creatinine (Cre), heavy metals, caffeine, and dopamine[13][14][15][16][17]. In the past years, a few studies had also been conducted using the 3D printing technology for uric acid detection[18–20]. These studies exhibit limitations like miniaturization of the devices, labor-intensive processes, and high operational costs. Thus, extending the 3D printed sensing platform to integrate with portable devices is necessary for a significant research direction to offer higher sensitivity, rapid response, low cost, portability, and real-time response over other conventional technologies [21–23].

View Article Online
DOI: 10.1039/D6SD00005C

Several studies suggest that increasing the surface area of the device and utilizing various nanomaterials for sensor signal amplification can enhance electrochemical signals[24–26]. Among those, the use of gold nanoparticles[27], graphene oxide[28,29], and metal oxide nanomaterials such as CuO, MnO_2, TiO_2, and Ce_3O_4[30][31][32] has increased the selectivity and sensitivity of the non-enzymatic biosensing applications[16,33–35]. Despite these advanced techniques, conventional UA sensors based on enzymatic and non-enzymatic methods still face difficulties, such as a low detection limit, limited portability, high sample volume requirements, poor stability, and reduced reproducibility, with restricted application for point of care testing [12,17,36].

Herein, miniaturized 3D CPE electrochemical devices have been fabricated for uric acid detection. The fabricated devices were modified with DMF to increase porosity, followed by carboxylate multiwalled carbon nanotubes (MWCNTs) to enhance conductivity and electrocatalytic activity for uric acid detection. The material modification was confirmed by the SEM, EDAX, and FTIR characterization techniques. The enzymatic approach was employed to detect using the uricase enzyme with the specific linker. The electrochemical optimization and characterization, including electrocatalytic activity, pH effect, concentration, interference, repeatability, and reproducibility of the developed microelectrode, were carried out, and it was integrated with a portable potentiostat. Importantly, its performance was also validated using a human serum sample, achieving significant recovery values (97%), within the clinically acceptable range, thereby confirming its suitability for real sample analysis and point of care application in diagnostic testing.

2. Materials and methods

2.1 Materials

All chemicals were of analytical grade. Uric acid (UA), L-Ascorbic acid (AA), potassium chloride (KCl), potassium ferricyanide [$K_3Fe(CN)_6$], Uricase enzyme from Candida sp. (250 U) from Sigma Aldrich, India, sodium phosphate monobasic ($NaH_2PO_4 \cdot H_2O$), L-tryptophan (LP), sodium phosphate dibasic ($Na_2HPO_4 \cdot H_2O$), glucose, sodium chloride (NaCl), and creatinine (Cr), all with a purity of approximately 99.9%, were used and purchased from Sigma Aldrich, India. Multiwalled carbon nanotubes (MWCNTs) were procured from TCI India. Dimethylformamide (DMF) [$HCON(CH_3)_2$] was used as an organic solvent for electrode-surface activation. EDC (1-ethyl-3-(3-dimethylaminopropyl)carbodiimide) and NHS (N-

View Article Online
DOI: 10.1039/D6SD00005C

hydroxysuccinimide) were obtained from Sigma-Aldrich, India. All solutions were prepared using deionized water with a resistivity of 18.2 MΩ·cm.

2.2 Instruments

Various instruments were utilized for device fabrication and electrode characterization. The electrochemical device characterization was carried out using the potentiostat, model SP-150 potentiostat and portable Sensit BT potentiostat were purchased from BioLogic Science Instruments (France) and Sensit BT, Palmsens (Netherlands). A Dual extruder 3D printer from BCN3D (SIGMA D25 model) from (Lleida, Spain). Scanning electron microscopy (SEM) was used for surface morphology study was procured from (Apreo SEM from Thermo Fisher Scientific, USA). An electrically conductive composite polylactic acid (PLA) filaments (2.85 mm, black color) were purchased from Protopasta 3D filaments (Vancouver, USA). The pH measurement was carried out using a double junction pH meter procured from (Oakton 700 pH electrode, Singapore). A Silver-silver chloride (Ag/AgCl) paste procured from ALS, Japan. non-conducting polylactic filament (PLA) was also purchased from BCN3D Filaments (Lleida, Spain).

2.2 Design and fabrication of 3D Printed conductive electrodes

The electrode geometry was designed in SolidWorks (Student Version 2024) and exported in stereolithography (.stl) format, followed by a slicing software, to print geometry (G code), as shown in Fig 1 (a & b). The device was printed by fused deposition modeling (FDM) based 3D printing approach using a dual extrusion 3D printer with 0.4 mm nozzles, operating at 210 °C. A non-conductive PLA filament was used to form the base structure. In contrast, a carbon-loaded conductive PLA filament was used to print the integrated three electrode system, comprising a working electrode (WE), a reference electrode (RE), and a counter electrode (CE), as shown in Fig 2 (a, b & c). The final printed electrode had a rectangular footprint of 25 mm × 11 mm, with a thickness of 0.5 mm. A 5 mm × 5 mm sample reservoir was incorporated into the design to confine the analyte solution. Post fabrication, the printed electrodes were treated with dimethylformamide (DMF) for 5 minutes to enhance surface wettability and electrocatalytic activity, followed by rinsing with deionized (DI) water and air drying. The DMF treatment induces swelling and partial dissolution of the PLA matrix, leading to exposure of embedded conductive fillers and formation of micro-/nano-porous structures upon solvent evaporation, thereby enhancing the effective electroactive surface area. Similar solvent-induced morphological modifications in polymer composites. Each print cycle produced 20 identical sensor devices in a single run using the dual-extrusion 3D printer.

View Article Online
DOI: 10.1039/D6SD00005C

All 20 electrodes from a given print were subjected to the same surface modification and functionalization protocol in batch (identical reagent volumes, incubation times, and washing steps). To minimize electrode-to-electrode variability, all printing parameters were kept constant across batches: printing speed (50% of the printer's rated speed), nozzle temperature (220 °C), layer height, infill density, and extrusion flow rate.

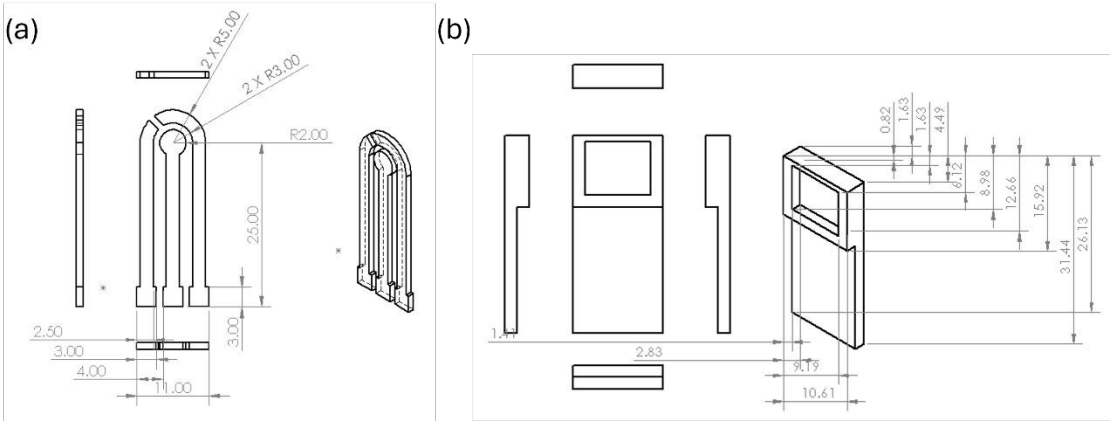

Fig 1. (a) The dimensions of the developed three electrode (b) front view, side view, and back view of the microelectrode with the dimensions.

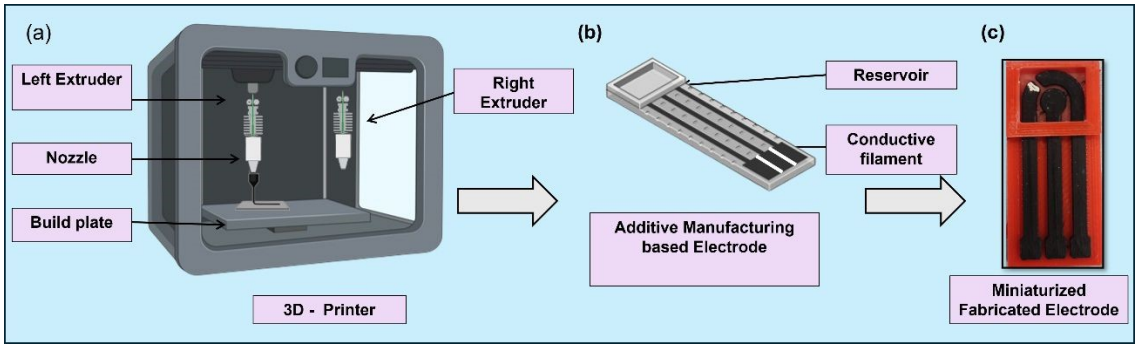

Fig 2. (a) The fabrication of an electrochemical sensor using carbon conductive electrodes using the 3D printing (BCN 3D Printer), (b) Printed electrode with the sample reservoir and conductive electrodes using additive manufacturing, and (c) the final fabricated miniaturized electrodes.

2.3 Analyte and Enzyme Preparation

All solutions were prepared in a freshly prepared 0.1 M phosphate buffer solution (pH 7.0) to support the entire electrolyte for voltammetry and chronoamperometric detection of uric acid. The stock solution of uric acid was prepared in 0.1 M PBS, and the various concentrations were obtained by diluting the stock solution. The uricase enzyme was also prepared in 0.1 M PBS (pH 7), where the uricase was taken as 1 mg in 1 mL of PBS, a freshly prepared solution

View Article Online
DOI: 10.1039/D6SD00005C

during the experimental procedure. Additionally, the multiwalled carbon nanotube was prepared using 10 mg of MWCNT powder in 1 mL of ethanol (99% pure). A 30:10 ratio of EDC and NHS was also used for electrode modification to activate the electrode surface with carboxyl groups, which can then be used for the covalent binding of uricase enzymes.

2.4 Sensing mechanism

The electrochemical sensing mechanism for uric acid was facilitated through a biocatalytic mechanism, using uricase enzymes, immobilized onto a 3D-CPE printed electrode surface. The working was modified with multiwalled carbon nanotube (MWCNTs) to increase the electroactive surface area of the electrode and electron transfer. EDC and NHS were employed on the electrode surface area to enhance the immobilization of the uricase enzyme and facilitate its proper binding. The uricase enzyme catalyzes the oxidation of uric acid to allantoin, with the production of hydrogen peroxide (H_2O_2), and the generated H_2O_2 and carbon dioxide (CO_2); the reaction mechanism is shown below in equation (1).

$$\text{Uric Acid} + O_2 + H_2O \xrightarrow{\text{Uricase}} \text{Allantoin} + CO_2 + H_2O_2 \qquad (1)$$

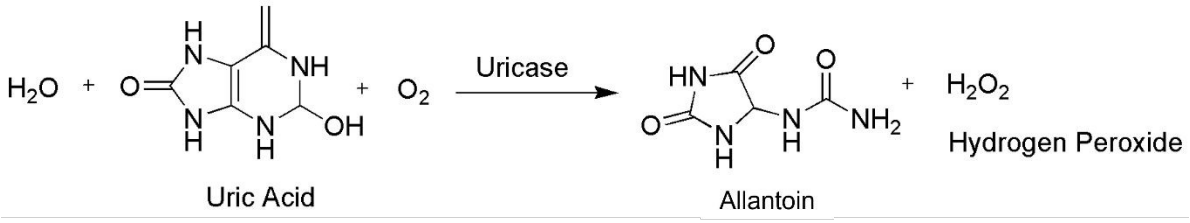

The generated H_2O_2 is electrochemically active and undergoes further oxidation at the electrode surface, producing a measurable current response proportional to the uric acid concentration.

2.5 Electrode Modification

The electrode modification was carried out using dropcasting techniques. Initially, the electrode was treated with a 0.1 M solution of dimethylformamide (DMF) to increase the porosity of the work

ing electrodes. Later, a 10 mg/mL solution of carboxylated multiwalled carbon nanotubes (MWCNTs) was prepared in pure ethanol (99.99%) and kept in a water bath to facilitate dispersion of the solution. Afterward, the crosslinker was prepared in a 30:10 ratio of 0.2 M EDC and 0.05 M NHS, dissolved in 0.1 M PBS (pH 7). A volume of 20 µL was dropcasted after MWCNT modification. Finally, the uricase enzyme was prepared in a 1 mg/mL solution of PBS (pH 7). A 10 µL volume of the prepared solution was drop casted on the working electrode area and kept at 4 °C overnight, as depicted in Fig (3). Subsequently, all the electrochemical detections were carried out.

View Article Online
DOI: 10.1039/D6SD00005C

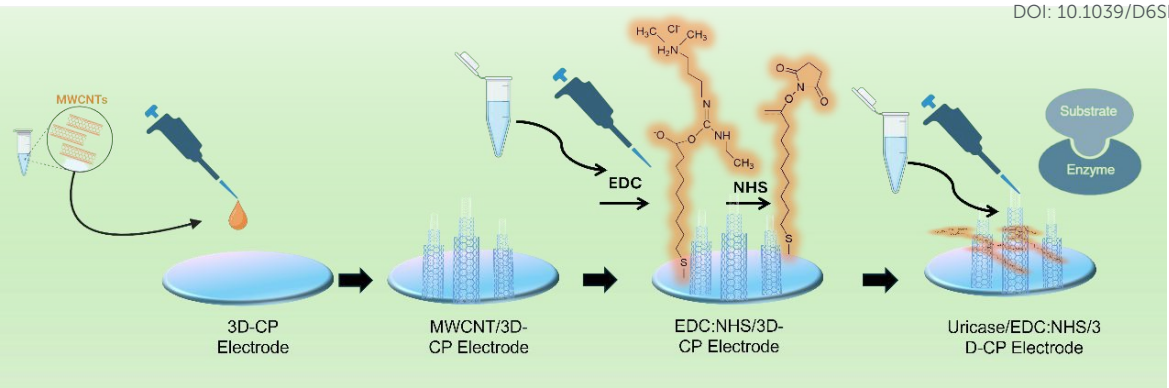

Fig 3. Schematic diagram for the stepwise electrode surface modification for uric acid (UA) detection.

3. Results and discussion

To test the performance of the sensor and structural features of the developed miniaturized devices, including their structural properties and electrochemical performance, of the 3D-CPE biosensor. The morphological characterization of the sensor was carried out using SEM, EDX, and FTIR to confirm the electrode functionalization. The electrochemical characterization was carried out using cyclic voltammetry (CV) and chronoamperometry (CA) techniques.

3.1 Material Characterization

To understand the electrode characterization upon each successful stepwise modification for the 3D-CPE devices. Scanning electron microscopy (SEM), Energy Dispersive X-ray Spectroscopy (EDX), and modification of the functional group at each stage were carried out using Fourier transform infrared spectroscopy (FTIR). All the elaborative studies are presented in the section below.

3.1.1 FE-SEM Analysis

Morphological studies of the electrode surface area were conducted using field-emission scanning electron microscopy (SEM). Initially, the samples were kept for gold coating using gold coater instruments for each of the samples prepared, up to 15 nm. As shown in Fig 4 (a), bare 3D-CPE was conducted, which exhibits a relatively limited microstructural feature. As shown in Fig 4 (b), DMF treated electrodes show a rougher and more porous surface morphology, characterized by increased surface texture and microvoids. Figure 4 (c) and (d) shows, the modification with multiwalled carbon nanotubes, which are evenly distributed on the electrode surface, with magnifications of 10 µm and 500 nm [37]. These results show an increase in surface area and a change in porous nature with modification, which benefits the electrochemical sensor application.

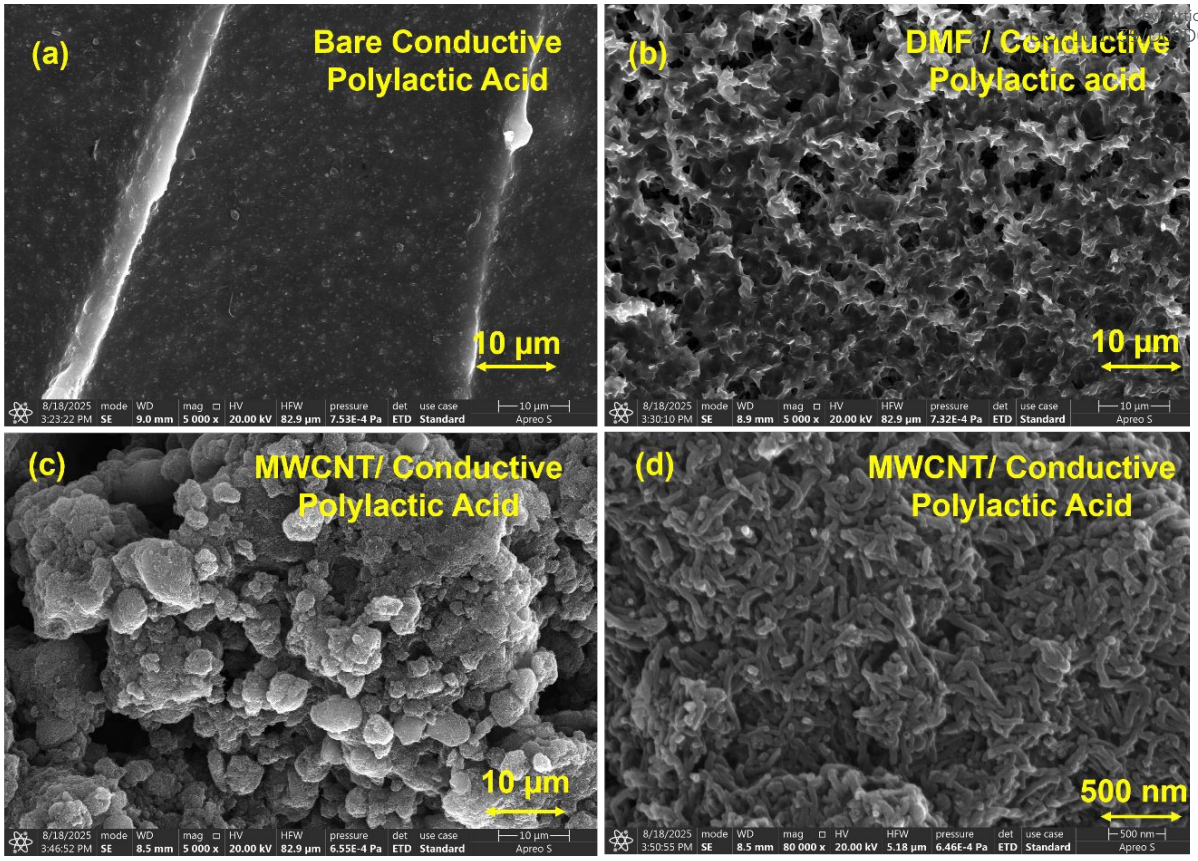

Fig. 4. FE-SEM images of the working electrode shown in (a) bare 3D-CPE at magnification of 10 µm, (b) DMF treated 3D-CPE, at the magnification of 10 µm, showing the increased surface porous nature, and in figures (c) and (d) 3D-CPE modified with the MWCNTs were successfully modified with the magnification of 10 µm and 500 nm.

3.1.2 EDX Analysis

The elemental composition of the modified material was confirmed using Energy dispersive X-ray spectroscopy (EDX), which was employed to analyze the 3D-CPE device at each stage of surface modification. As shown in Fig 5 (a) and (d), the bare 3D-CPE, having an elemental composition of carbon (C) and oxygen (O), presents atomic percentages of 80.65% and 19.35%, respectively, with a carbonaceous base structure. In Fig 5 (b) and (e), the electrode surface was modified with DMF, and the elements present were C, O, Si, and S, which are additional elements, with atomic percentages of 80.27%, 18.95%, 0.38%, and 0.40%, respectively. In Fig 5 (c) and (f), the modification of the MWCNTs shows an increase in the atomic percentage of carbon elements to 91.68% and a decrease in the oxygen elements to 8.32%, indicating that the increased percentage of elements leads to better electrochemical studies.

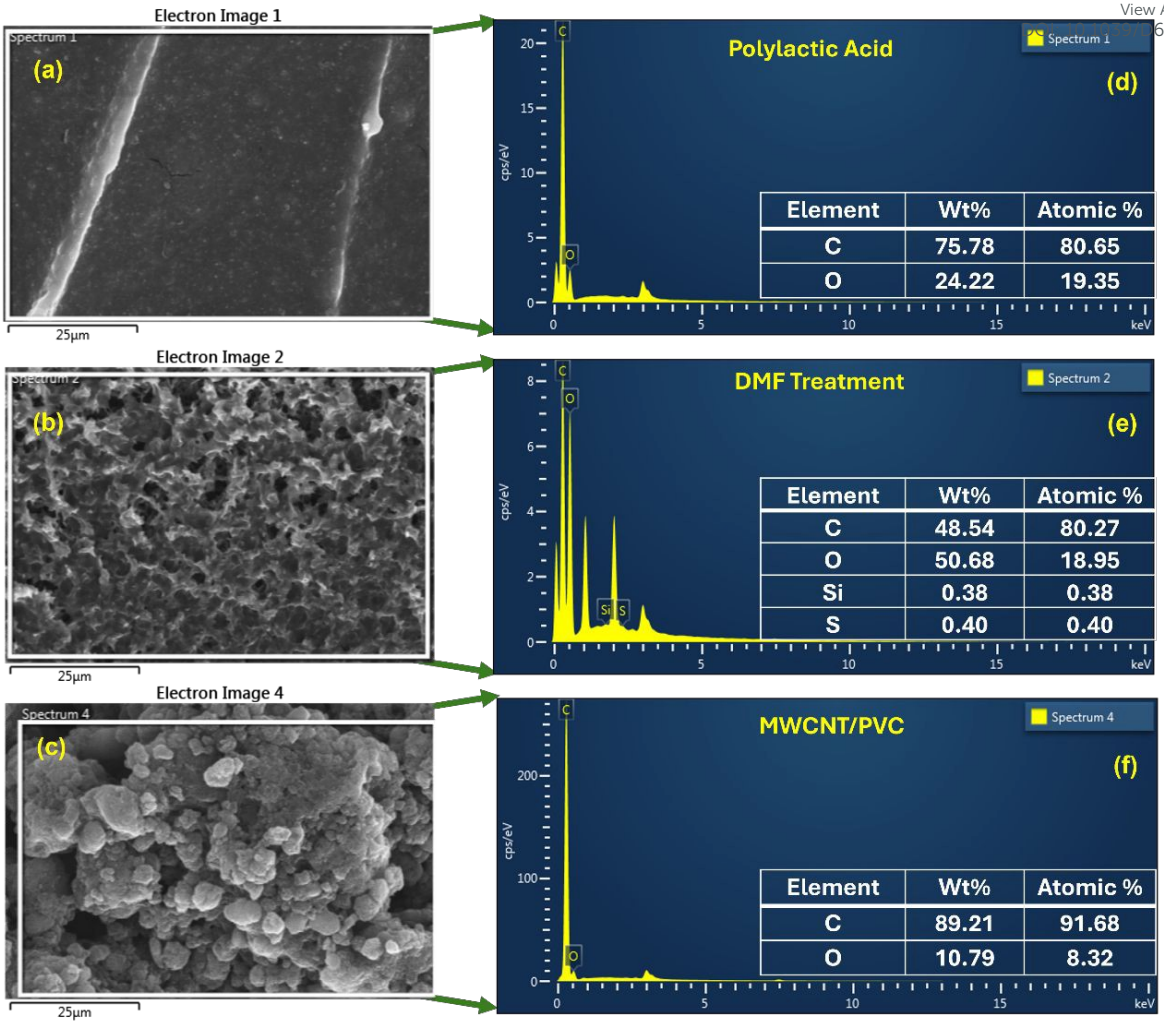

Fig. 5 EDX analysis for the (a) and (d) for the bare 3D-CPE, inset table showing the elemental composition for the C, and O. (b) and (e) shows DMF treated 3D-CPE inset the elemental composition depicting C, O, Si, and S and (c) and (f) shows MWCNT-coated 3D-CPE and inset all the elemental percentage.

3.1.3 XPS Analysis

X-ray photoelectron spectroscopy (XPS) analysis was performed to confirm the elemental composition and chemical states of the 3D-CPE. The XPS survey for the 3D-CPE confirms the presence of the elements C and O, as shown in Fig 6 (a). The presence of the C 1s spectrum, as shown in Fig 6 (b), confirms a peak at 284.8 eV for C-C. Subsequently, fitting was carried out using Avantage software (Thermo Fisher Scientific) to verify the deconvolution of the carbon elements at the peak for C-O-C at 286 eV. The O-C=O peak at 288.5 eV indicated the graphitic structure, and the functional group helps to enhance electron transfer and provide proper immobilization. The O 1s XPS spectrum as shown in Fig 6 (c), of the modified electrode was deconvoluted into two main components centered at ~531.8 eV

View Article Online
DOI: 10.1039/D6SD00005C

and ~533.3 eV. The peak at ~531.8 eV is assigned to C=O groups, including carbonyl and amide functionalities, indicating the formation of covalent linkages between the carboxyl groups of MWCNT and amine groups of uricase via EDC/NHS coupling. The second component at ~533.3 eV corresponds to C–O/O–C–O species, arising from hydroxyl or epoxy groups present on the carbon surface. A minor high binding energy tail (~534 eV) is also observed, which is attributed to adsorbed water or oxygen species[38]. These bonds, as presented in the XPS survey, will help improve hydrophilicity and charge transfer, enhancing electrochemical sensing.

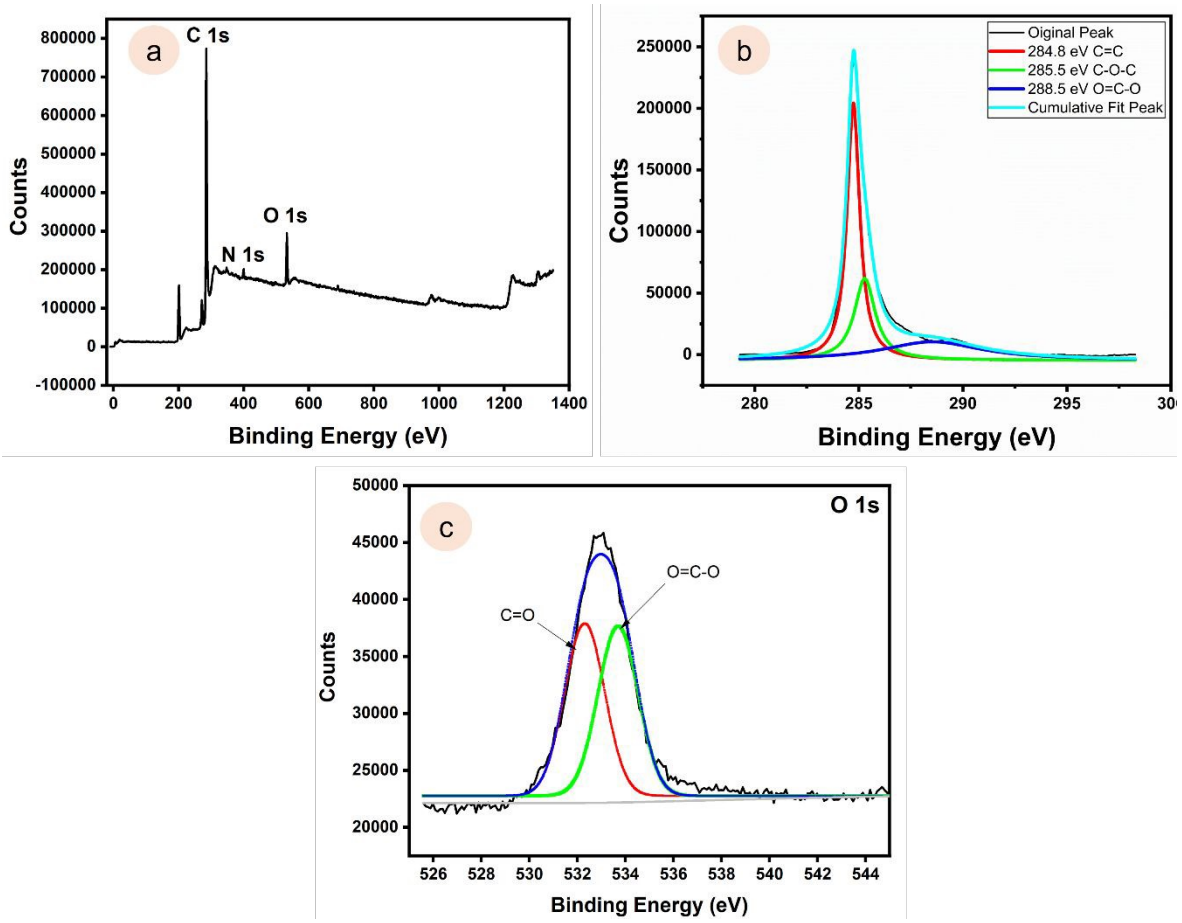

Fig. 6 XPS analysis of the 3D-printed carbon-conductive polylactic electrode (3D-CPE): (a) full survey spectrum showing the presence of C 1s and O 1s peaks, (b) high resolution C 1s spectrum deconvoluted into C–O–C and O–C=O at 284.8 eV, and (c) O 1s high-resolution XPS spectrum showing deconvoluted peaks at ~531.8 eV and ~533.3 eV, corresponding to C=O and C–O/O–C–O functional groups, respectively.

3.1.4 Fourier Transform Infrared Spectroscopy (FTIR) Analysis

Fourier Transform Infrared Spectroscopy was employed to confirm the sequential surface modifications of the 3D electrode during fabrication. The FTIR spectrum of the DMF treated

View Article Online
DOI: 10.1039/D6SD00005C

electrode exhibited characteristic peaks around 1640 cm^{-1} and 1400 cm^{-1}, corresponding to C=O stretching (amide) and C–N bending vibrations, respectively, indicating partial surface activation and interaction of DMF with the electrode matrix, as shown in Fig 7. Upon modification with multiwalled carbon nanotubes (MWCNTs), a prominent peak at approximately 1570 cm^{-1} was observed, attributed to C=C stretching vibrations from the graphitic backbone of MWCNTs, along with a broad O–H stretching band around 3400 cm^{-1}, indicating the presence of hydroxyl groups from surface oxidation. Subsequent activation using EDC/NHS chemistry introduced new peaks near 1740 cm^{-1} and 1380 cm^{-1}, which were assigned to ester C=O stretching and N–O symmetric stretching, respectively. These peaks are characteristic of the successful formation of NHS esters and confirm the activation of carboxyl groups for amide bond formation. Finally, after uricase immobilization, two new bands emerged at ~1655 cm^{-1} and ~1540 cm^{-1}, corresponding to the amide I (C=O stretching of the peptide bond) and amide II (N–H bending and C–N stretching) vibrations, respectively, which are indicative of protein secondary structure and confirm the successful covalent attachment of the enzyme on the electrode surface.

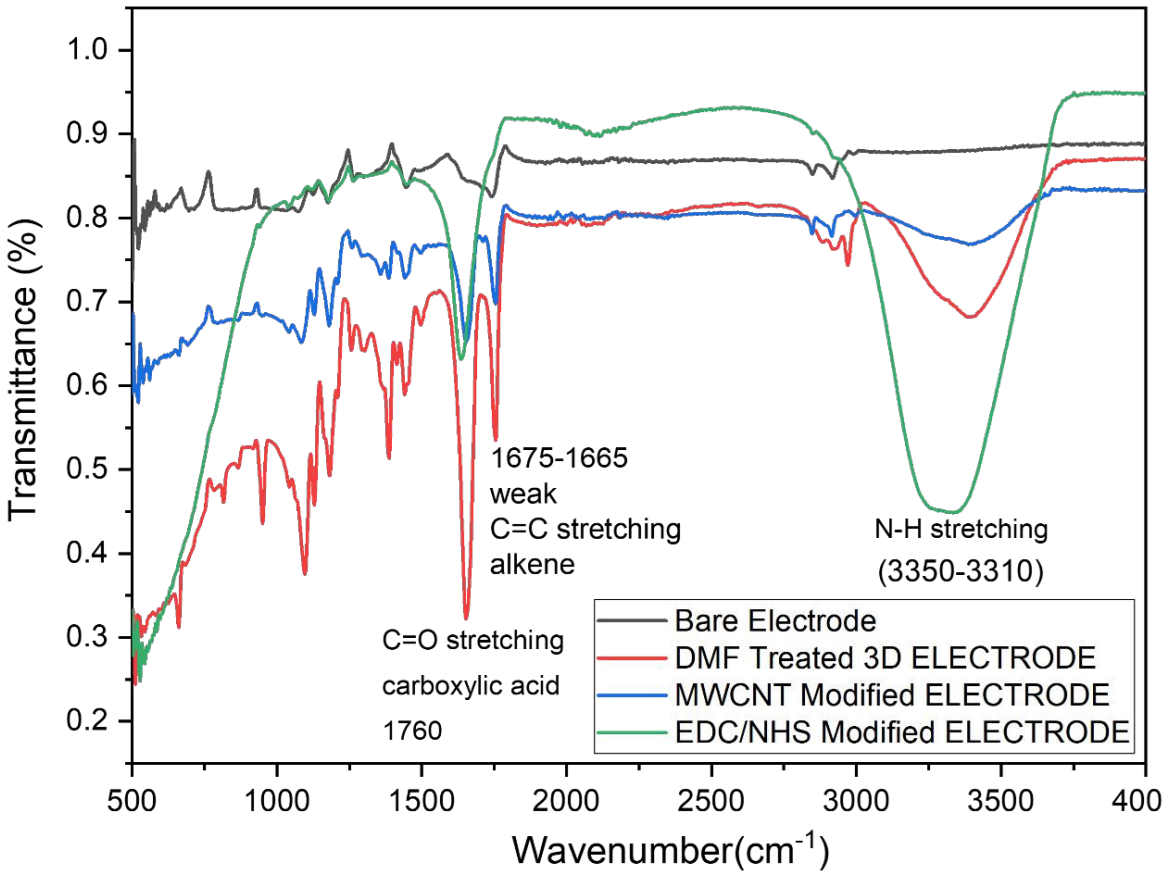

View Article Online
DOI: 10.1039/D6SD00005C

Fig. 7 FTIR spectra of the 3D electrode at different stages of surface modification: bare electrode, DMF-treated electrode, MWCNT modified electrode, EDC/NHS activated surface, and Uricase immobilized electrode. Characteristic peaks corresponding to functional groups confirm the successful stepwise modification and enzyme immobilization.

3.2 Analytical performance of 3D-CPE printed electrode towards Uric Acid

3.2.1 Electrochemical behaviour of the device using a redox mediator

The Cyclic voltammetry (CV) was performed using a standard 5 mM $[Fe(CN)_6]^{3-/4-}$ redox probe in 0.1 M KCl to evaluate the electrochemical activity and electron transfer kinetics of the 3D-CPE electrode at various stages of modification. The bare electrode exhibited well-defined redox peaks with a moderate peak-to-peak separation (ΔEp), indicating quasi-reversible behaviour. Upon modification with MWCNTs, a significant increase in peak current and a decrease in ΔEp were observed, suggesting enhanced electron transfer due to the nanotube high conductivity and increased surface area. Further functionalization with EDC/NHS and uricase resulted in a slight decrease in peak current, attributed to partial electrode surface blocking by the biomolecular layer, as shown in Fig 8 (a). These results confirm the successful modification of the electrode and the preservation of electrochemical activity necessary for biosensing applications.

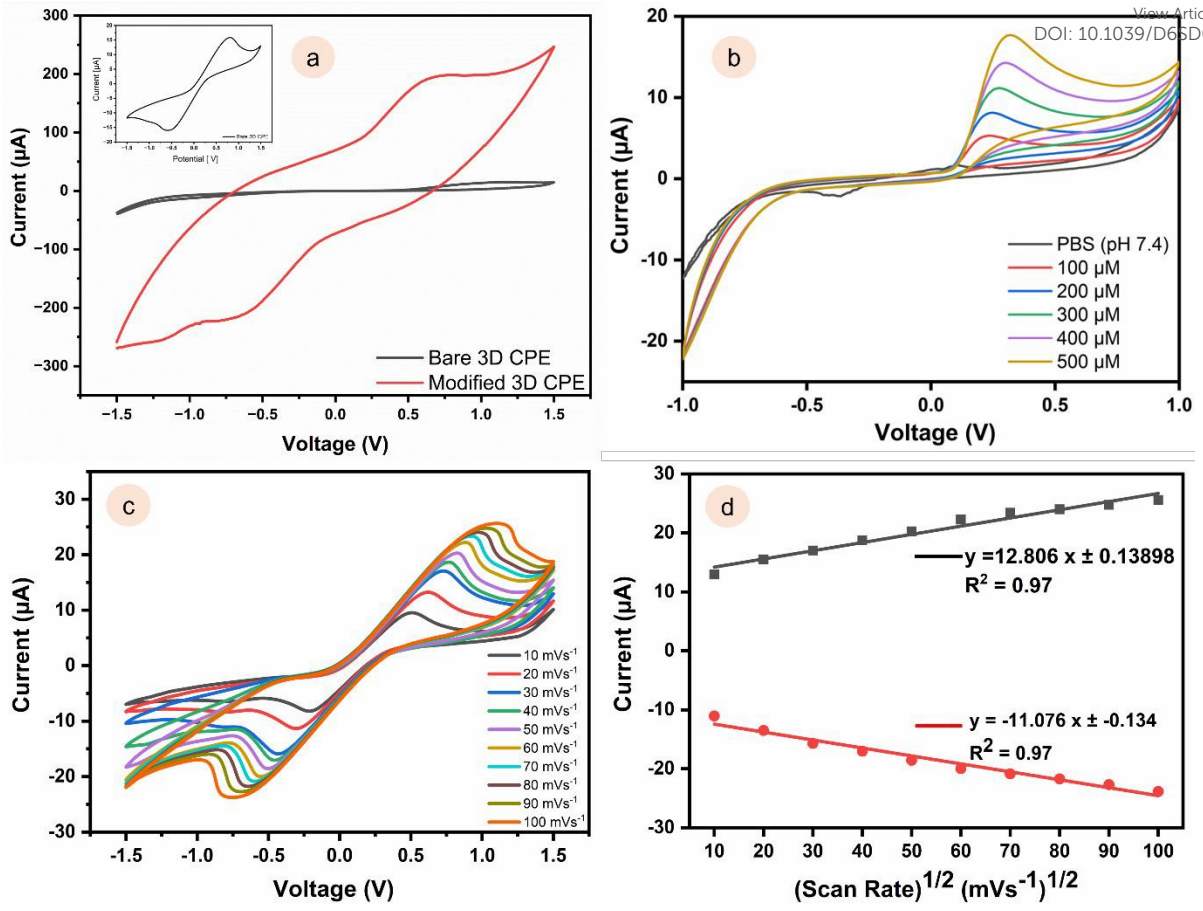

Fig. 8 (a) CV of 3D CPE electrode for the device performance using 5 mM $K_3[Fe(CN)_6]$ in 1 M KCl solution. (a) Inset figure for the bare 3D CPE electrode in the range of -1.5 to 1.5 V at the 50 mV/s. (b) CV response of electrodes in the presence PBS (pH 7) and (1000 µM) Uric acid at 50 mV/s at the electrode surface of Uricase/MWCNT/3D printed carbon conductive filament based electrode (3D-CPE). (c) CV responses of various scan rates on uric acid detection from 10 mVs^{-1} to 100 mVs^{-1}. (d) Corresponding calibration curve plot for the I_{pa} Vs (Scan rate)$^{1/2}$ $(mVs^{-1})^{1/2}$.

3.2.2 Optimization of pH effect study for Uric Acid

The effect of pH on the electrochemical response of uric acid was investigated using cyclic voltammetry (CV) in 0.1 M phosphate buffer (pH 3–10) containing 500 µM uric acid. CV study shows a strong pH dependence due to the proton occurring in the redox mechanism. At pH (3–5), redox peaks, with low current observed, are attributed to protonation of uric acid and hindered electron transfer. Increasing the pH from 6 to 9 resulted in enhanced anodic currents and a negative shift in oxidation potential, consistent with a proton coupled electron transfer (PCET) process. At pH 7, well defined redox peaks with maximum current response were obtained, indicating optimal electron transfer kinetics and molecular stability. Beyond

View Article Online
DOI: 10.1039/D6SD00005C

pH 9, peak broadening suggested uric acid instability in alkaline media. Therefore, pH 7 was selected as the optimal working condition, providing both physiological relevance and stable electrochemical performance.

3.2.3 Cyclic Voltammetry Responses of Uric Acid

The electrochemical behaviour of the device was tested with 1 mM of 50 µL uric acid solution by the CV in 0.1 M Phosphate buffer solution (PBS) of pH 7 in the optimized potential window of 1 V to -1 V with the scan rate of 50 mV/s, and sample volume is 50 µL. The CV response was recorded for the bare 3D-CPE and Uricase/EDC/NHS/MWCNT/Modified 3D printed carbon conductive filament based electrode (3D-CPE) with the PBS and in the presence of the uric acid at the scan rate of the 50 mV/s, as depicted in the Fig 8 (b). The response for the bare 3D CPE for the uric acid, there was no significant peak were observed, whereas for the modified Uricase/EDC: NHS/MWCNT/Modified 3D CPE electrode a significant oxidation peak was observed at 0.31 V as per by the reported works which indicated that uric acid undergoes oxidation with the developed device[20,27,31,39].

3.2.4 Effect of Scan Rate Study

Cyclic voltammetry was performed at varying scan rates ranging from 10 to 100 mV s^{-1} in the presence of 0.5 mM $K_3[Fe(CN)_6]^{3-/4-}$ in 1 M KCl within the potential window of –1.5 to +1.5 V, as shown in Fig 8 (c). The ferri/ferrocyanide redox couple exhibited well defined anodic and cathodic peaks, both of which increased proportionally with the square root of the scan rate, confirming diffusion controlled electron transfer. The corresponding calibration plots of anodic and cathodic peak currents versus the square root of scan rate displayed linear relationships, as shown in figure 8 (d). This behaviour is consistent with the Randles–Ševčík equation for reversible systems:

$$I_{pa} = 2.69\times10^{5}\, n^{3/2} A D^{1/2} C\, v^{1/2} \qquad (1)$$

where, $I_{pa}/v^{1/2}$ is the slope calculated from the calibration graph 12.806 µA/$(mVs^{-1})^{1/2}$, n the number of electrons participated in the reaction (assumed to be 1), The geometric area of the working electrode (WE), based on a 4 mm diameter, was calculated to be 0.126 cm^2. Using this value, the diffusion coefficient (D) was determined using the Randles–Ševčík equation, the calculated diffusion coefficient was found to be (D) ($cm^2\ s^{-1}$) = 5.74 × 10^{-7} cm^2/s, C the analyte concentration (mol cm^{-3}) = 0.5 mM, and v the scan rate (mVs^{-1}). which is in reasonable agreement with reported values for the ferri/ferrocyanide system, confirming the reliability of the electrochemical response. The strong linearity indicates that the fabricated electrode provides efficient and stable electron transfer characteristics.

View Article Online
DOI: 10.1039/D6SD00005C

3.2.5 Effect of Concentration Study

To evaluate the sensitivity and analytical performance of the developed sensor, the uric acid concentration dependent electrochemical response was studied using the chronoamperometric (CA) technique. The measurements were conducted under optimized conditions at an anodic potential of 0.31 V (determined from cyclic voltammetry) for 60 s, with a sample volume of 50 µL. The concentration study was carried out in the range of 10 to 500 µM, as shown in Fig 9 (a). A gradual increase in current response was observed with increasing uric acid concentration, confirming the efficient catalytic oxidation of uric acid by the uricase modified 3D printed carbon conductive filament based electrode (3D-CPE). This reaction indicates the proper electrocatalytic activity of uric acid to allantoin, carbon dioxide, and hydrogen peroxide (H_2O_2), where uricase, as the enzyme used, is described by the following enzymatic reaction mechanism.

Uric acid $+ O_2 + H_2O \xrightarrow{\text{Uricase}}$ Allantoin $+ CO_2 + H_2O_2$The generated hydrogen peroxide (H_2O_2) undergoes electrochemical oxidation at the electrode surface, producing an anodic current proportional to the uric acid concentration.

$H_2O_2 \rightarrow 2H^+ + O_2 + 2e^-$This redox process behaviour of the device mechanism, where the current increase reflects the oxidation of enzymatically produced H_2O_2. The calibration plot with the correlation coefficients of $R^2 = 0.99$), indicating proper linearity as shown in Figure 9 (b). Based on the slope and standard deviation (σ) of the calibration curve, the limit of detection (LOD) and limit of quantification (LOQ) were calculated using the equations [40,41].

$$\text{LOD} = 3.3 \times \frac{\sigma}{S} \qquad (2)$$

$$\text{LOQ} = 10 \times \frac{\sigma}{S} \qquad (3)$$

The calculated LOD and LOQ values were 7.95 µM and 24.11 µM, respectively, demonstrating the capability of the sensor for trace level detection of uric acid.

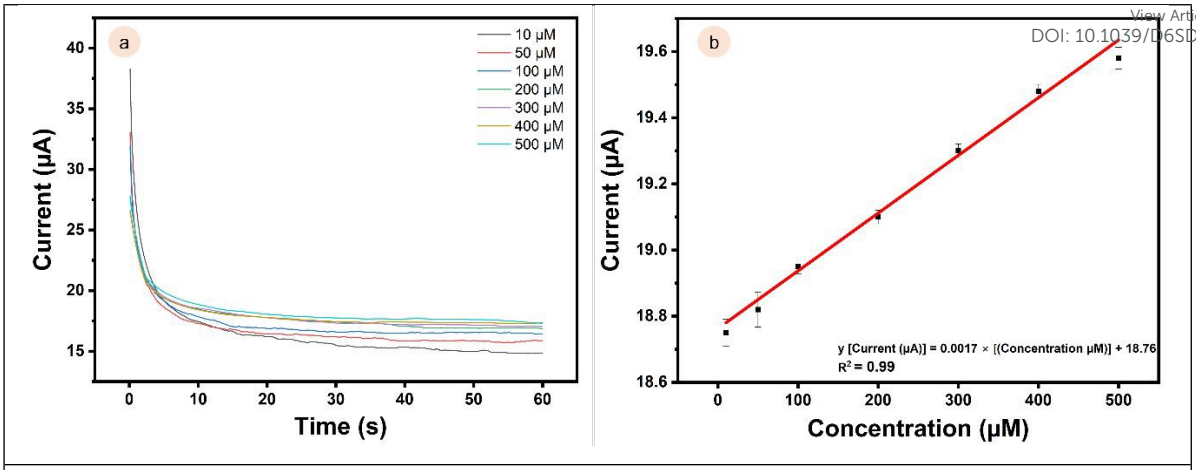

Fig. 9 (a) Chronoamperometric response of the uricase modified 3D (3D-CPE) recorded at different uric acid concentrations (10–500 µM) under an applied potential of 0.31 V for 60 s. (b) Corresponding calibration plot showing a linear relationship between current response and uric acid concentration ($R^2 = 0.99$).

3.2.6 Interference study

The selectivity of the uricase modified 3D-CPE sensor was investigated toward 100 µM uric acid in the presence of physiologically relevant interferents, including creatinine (50 µM), ascorbic acid (10 µM), urea (100 µM), lactate (1 mM), glucose (5 mM), K^+ (4 mM), and Na^+ (130 mM). Chronoamperometric (CA) measurements were performed in 0.1 M phosphate buffered saline (PBS, pH 7) at an applied potential of +0.31 V for 60 s using a sample volume of 100 µL. As shown in Fig 10 (a), the current response for uric acid exhibited negligible variation after the sequential addition of these potential interferents, with a relative standard deviation (RSD) of 3.5%. These results demonstrate that the developed biosensor possesses excellent selectivity toward uric acid detection, even in the presence of coexisting electroactive or ionic species.

View Article Online
DOI: 10.1039/D6SD00005C

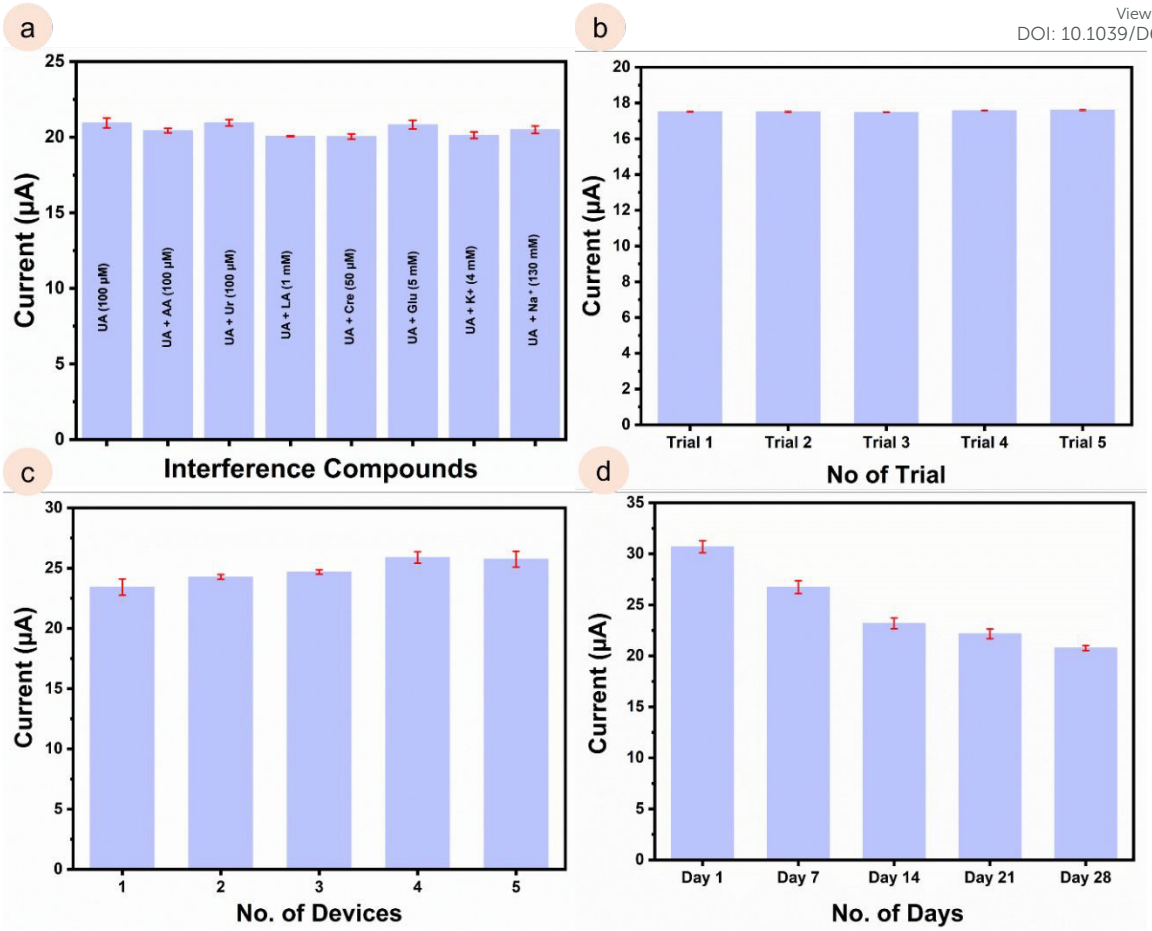

Fig. 10 (a) Chronoamperometric (CA) responses of the uricase modified 3D-CPE sensor toward 100 μM uric acid in the presence of potential interferents, including creatinine, ascorbic acid, urea, lactate, glucose, K^+, and Na^+ ions, recorded in 0.1 M PBS (pH 7) at +0.31 V for 60 s. (b) Repeatability study was carried out using chronoamperometric responses of a single uricase modified 3D-CPE for ten successive additions of 300 μM uric acid in 0.1 M PBS (pH 7) at +0.31 V, showing highly consistent currents (RSD = 3.8%), (n = 3). (c) Reproducibility was carried out using five independently prepared uricase modified 3D-CPEs for 300 μM uric acid under identical conditions, demonstrating minor variations in current (RSD = 4.2%), (n = 3). (d) Storage stability was carried out using chronoamperometric response of the biosensor to 300 μM uric acid over 28 days, with electrodes stored at 4 °C in 0.1 M PBS, retaining ~92% of the initial current after two weeks, the experiments carried out in the triplets in numbers.

3.2.7 Repeatability, reproducibility, and stability of device

The repeatability of the uricase modified 3D-CPE sensor was evaluated using chronoamperometric (CA) measurements under optimized conditions. Ten successive

chronoamperometric responses were recorded for 300 µM uric acid in 0.1 M PBS (pH 7) at an applied potential of +0.31 V for 60 s. The current responses remained highly consistent, exhibiting a relative standard deviation (RSD) of 3.8%, confirming excellent signal repeatability as shown in Fig 10 (b). The negligible variation in current across repeated measurements indicates minimal electrode fouling and stable electron transfer kinetics at the modified electrode surface. To evaluate fabrication reproducibility, five independent Uricase modified 3D CPE electrodes were prepared using the same protocol. Their CA responses toward 300 µM uric acid were recorded under identical conditions. The oxidation peak currents showed only minor variations, with a relative standard deviation (RSD) of 4.2%, as shown in Fig 10 (c). This low RSD demonstrates reliable electrode preparation and consistent enzyme immobilization, essential for large scale sensor fabrication. The storage stability of the biosensor was evaluated by monitoring its chronoamperometric response to 300 µM uric acid at regular intervals over a 28 day period. When not in use, electrodes were stored at 4 °C in 0.1 M phosphate buffer (pH 7). The steady state current decreased gradually, retaining approximately 92% of the initial response after two weeks. This minimal loss indicates that both the enzymatic activity of uricase and the structural integrity of the modified electrode were well preserved under the storage conditions. The observed stability is comparable to or better than previously reported enzymatic biosensors, which typically exhibit a 10–15% decrease in activity over a similar period, as shown in Fig 10 (d).

3.2.8 Portable Device Validation

The concentration study was also carried out using a portable potentiostat (detail in the Equipment section) as shown in Fig 11 (a & b), Chronoamperometry techniques were carried out at an anodic potential of 0.31 V for 60 s, with a concentration range of 50 to 500 µM and a sample volume of 50 µL. The calculated linear response was observed in the range of 50 to 500 µM, and a coefficient of correlation of 0.98 was obtained, confirming linearity. The limits of detection and quantification were also calculated to be 7.4 µM and 22.4 µM, respectively. The portable Sensit BT potentiostat exhibits a higher LOD compared to the benchtop system, primarily due to its higher noise floor, lower current resolution, and limited amplifier sensitivity, which reduce the signal-to-noise ratio at low analyte concentrations. Despite this, the device demonstrates good linearity within the 50–300 µM range, which is relevant for practical point-of-care applications.

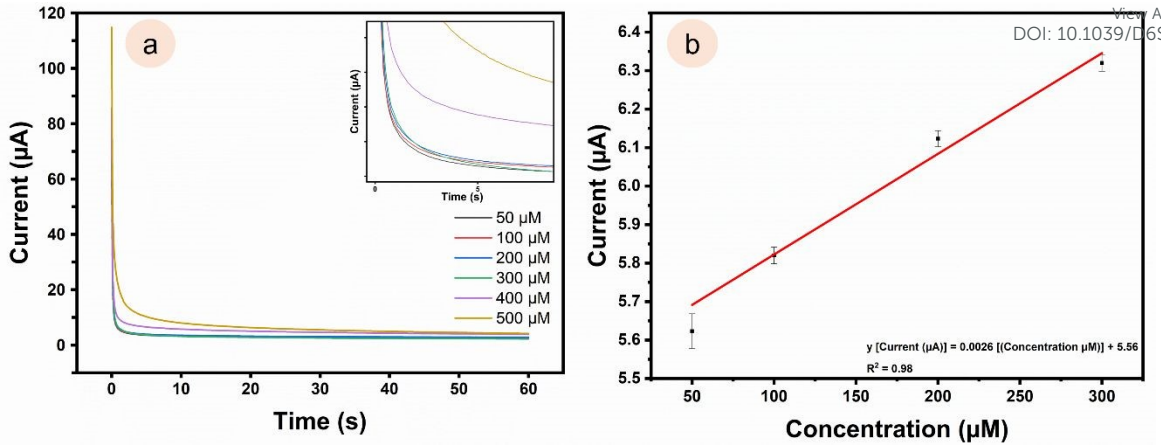

Fig. 11 (a) Concentration study using portable potentiostat in the range of 50 to 500 µM, as the inset figure shows the enlarged view, (b) corresponding calibration plot ($R^2 = 0.98$), the experiments carried out in the triplets in numbers (n = 3).

3.2.9 Real sample analysis

The practical applicability of the uricase modified 3D-CPE was demonstrated through chronoamperometric analysis of spiked human serum samples. Samples were diluted appropriately in 0.1 M PBS (pH 7), and CA measurements were carried out at an applied potential of +0.31 V. The known concentrations of uric acid were added to the samples, and the corresponding current responses were recorded, as shown in Fig 12 (a & b). The biosensor exhibited rapid, well defined, and concentration dependent currents, enabling accurate quantification. Recovery studies yielded values of 97% for serum samples, indicating excellent accuracy, as shown in Table 1. These results confirm that the enzymatic activity of uricase and the structural integrity of the modified electrode are maintained in complex biological matrices, highlighting the potential of the developed device for reliable clinical and diagnostic applications. A summary of previous studies on enzymatic electrochemical detection of uric acid is presented in Table 2.

View Article Online
DOI: 10.1039/D6SD00005C

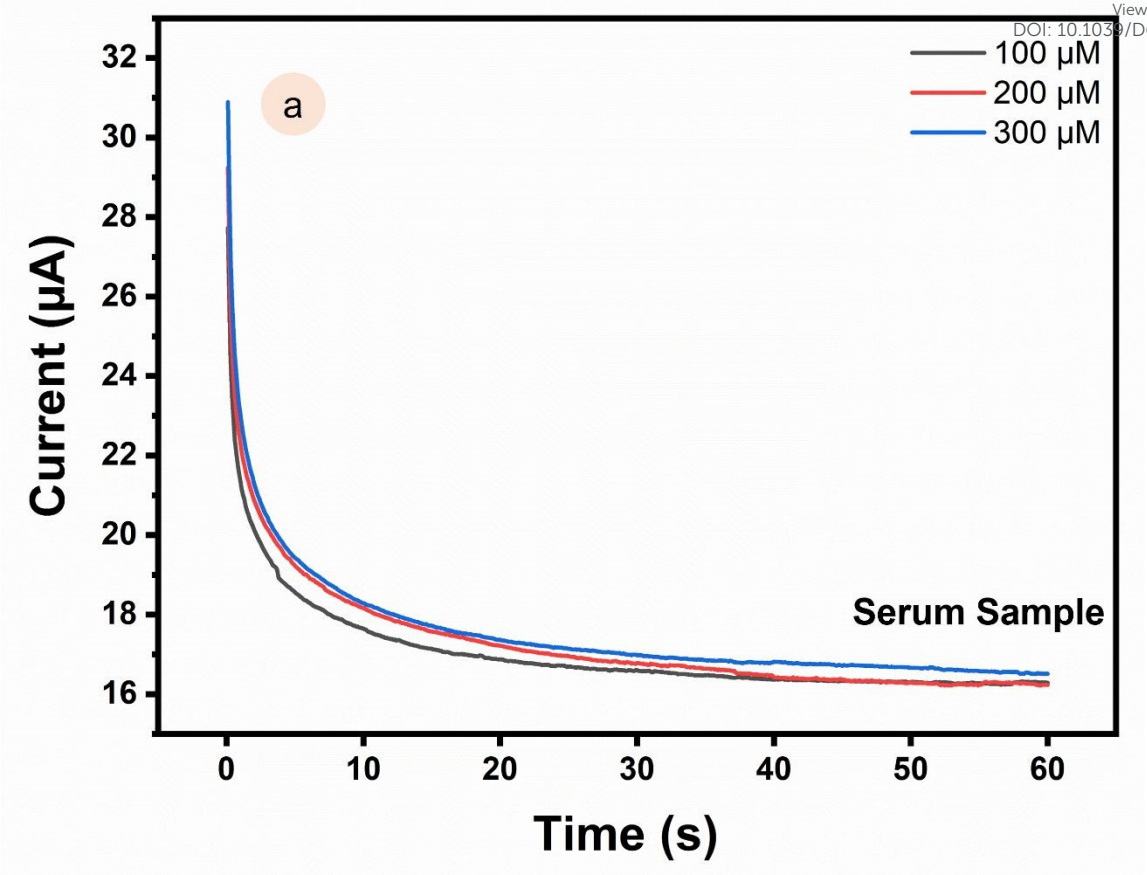

Fig 12. Chronoamperometric analysis of uricase modified 3D-CPE in real samples: (a) Human serum spiked with known concentrations of uric acid. The sensor exhibits rapid, concentration dependent current responses, with recoveries of 97% for serum demonstrating excellent accuracy and applicability in complex biological matrices.

Recovery percentage (%) = (Added / Found) ×100 [42–44]

Table 1. Real Sample Analysis

#	Sample	Added (µM)	Found (µM)	Recovery
1	Serum	100 µM	97.06	97.06 %
		200 µM	193.53	96.77 %
		300 µM	290.59	96.86 %

Table 2. An analytical performance of the present sensor compared with reported uric acid sensors.

#	Fabrication Techniques	Sensor Modification	Linear range (µM)	LOD (µM)	Portability/ Instrumentation	Ref

View Article Online
DOI: 10.1039/D5SD00005C

1.	Glassy Carbon Electrode	Nanotube paste electrode (enzymatic)	20 - 380	0.18	Benchtop system	[45]
2.	Glassy Carbon Electrode	CuO/GCE non-enzymatic sensor	1 - 400	0.6	Bulky System	[46]
3.	3D Printed	3D SACNT	100-1000	10	Benchtop	[47]
4.	Screen-Printed Electrode	AC/VCO/BW/SPE	10- 1000	43.8	Bulky System	[47]
5.	Screen-Printed Electrode	MC-ZnO/SPE	20 - 225	3.76	Bulky System	[48]
6.	Glassy Carbon Electrode	Fe_3O_4/GCE	20 - 160	14	Bulky System	[40]
7.	Carbon Paste Electrode	ZnO/PANI/CPE	10 - 120	7	Bulky System	[14]
8.	ECL	MoS_2 QDs	100 – 500	20	Benchtop System	[49]
9.	ITO	Uricase/CNT/Pani	100 – 1000	43.2	Benchtop System	[50]
10.	Glassy Carbon Electrode	AuNPs@MoS2	50 – 40000	10	Bulky system	[27]
11.	Carbon Conductive 3D-CPE	MWCNT/EDC/NHS/Uricase-modified 3D-CPE)	10 - 500	7.95 µM	Miniaturized PoC Devices (Sensit-BT Potentiostat)	This Work

View Article Online
DOI: 10.1039/D5SD00005C

Abbreviation: AuNPs : Gold Nanoparticles, ITO: Indium Tin Oxide, ECL: Electrochemiluminescence, ZnO: Zinc Oxide, MoS_2 : Molybdenum disulfide, CNT: Carbon nanotubes

4 Conclusion

This work presents a miniaturized and portable electrochemical device fabricated through a simple one step 3D printing approach for uric acid detection. A highly sensitive sensing platform was achieved by directly integrating working, counter, and reference electrodes from commercial conductive polylactic acid filaments and further functionalizing them with multi walled carbon nanotubes (MWCNTs), EDC/NHS coupling, and uricase. A well-defined oxidation potential at ~0.31 V was observed, and the device was systematically optimized with respect to pH, concentration, scan rate, interference, and stability. A wide linear range (10 – 500 μM) with an ultralow detection limit of 7.95 μM and a quantification limit of 24.11 μM was obtained. Finally, the real sample validation using serum samples (97%) and excellent recovery was observed. Meanwhile, reproducibility and stability studies confirmed the robustness of the platform. Collectively, a scalable, low sample volume, and low-cost route for the development of portable electrochemical biosensors was established, with strong potential for point of care testing (PoCT) of uric acid and broader applications in clinical diagnostics.

Acknowledgements

The authors gratefully acknowledge the financial support from the BITS BioCyTiH Foundation (Grant No. BBF/BITS(H)/FY2022-23/BCPS-114). The authors also thank BITS Pilani, Hyderabad Campus, for providing research infrastructure, and the Central Analytical Laboratory for access to characterization facilities.

All experiments were performed in accordance with the Guidelines of the Medical Centre at BITS Pilani, Hyderabad Campus and approved by the Medical Officer of the Medical Centre at BITS Pilani, Hyderabad Campus. Informed consents were obtained from human participants of this study.

References

[1] M. Kuwabara, T. Kodama, R. Ae, M. Kanbay, A. Andres-Hernando, C. Borghi, I. Hisatome, M.A. Lanaspa, Update in uric acid, hypertension, and cardiovascular diseases, Hypertens. Res. 46 (2023) 1714–1726. https://doi.org/10.1038/s41440-023-

View Article Online
DOI: 10.1039/D6SD00005C

01273-3.

[2] C.S. Kuo, C.M. Hwu, Y.H. Lin, Y.H. Huang, W.Y. Kao, M.J. Weih, L.C. Hsiao, C.F. Kwok, L.T. Ho, Portable electrochemical blood uric acid meter, J. Clin. Lab. Anal. 16 (2002) 109–114. https://doi.org/10.1002/jcla.10030.

[3] J.C. Chen, H.H. Chung, C.T. Hsu, D.M. Tsai, A.S. Kumar, J.M. Zen, A disposable single-use electrochemical sensor for the detection of uric acid in human whole blood, Sensors Actuators, B Chem. 110 (2005) 364–369. https://doi.org/10.1016/j.snb.2005.02.026.

[4] J.A. Muñoz, M. López-Mesas, M. Valiente, Development and validation of a simple determination of urine metabolites (oxalate, citrate, uric acid and creatinine) by capillary zone electrophoresis, Talanta. 81 (2010) 392–397. https://doi.org/10.1016/j.talanta.2009.12.014.

[5] Z.H. Sheng, X.Q. Zheng, J.Y. Xu, W.J. Bao, F. Bin Wang, X.H. Xia, Electrochemical sensor based on nitrogen doped graphene: Simultaneous determination of ascorbic acid, dopamine and uric acid, Biosens. Bioelectron. 34 (2012) 125–131. https://doi.org/10.1016/j.bios.2012.01.030.

[6] X. Chen, G. Wu, Z. Cai, M. Oyama, X. Chen, Advances in enzyme-free electrochemical sensors for hydrogen peroxide, glucose, and uric acid, Microchim. Acta. 181 (2014) 689–705. https://doi.org/10.1007/s00604-013-1098-0.

[7] F.W.L. Silva, B.R. Freire, C.S.C. Lopes, F.D. Marques, B.S. Archanjo, E.S. Ribeiro, R.E. Santelli, F.H. Cincotto, Cylindrical 3D-printed electrode based on carbon black and polylactic acid: an approach for electrochemical detection of the bithionol drug, Ionics (Kiel). 31 (2025) 6343–6352. https://doi.org/10.1007/s11581-025-06239-8.

[8] P.M. Kalligosfyri, C. Miller, S. Cinti, B.A. Patel, 3D printed electrode-microwell system: a novel electrochemical platform for miRNA detection, Microchim. Acta. 192 (2025). https://doi.org/10.1007/s00604-025-07190-1.

[9] L.S. Da Silva, L.R.G. Silva, H.S. Pittner, J.S. Stefano, D. Vanzin, R.M. Dornellas, B.C. Janegitz, L. V. de Faria, A. Galli, C.L. Handa, D.P. Rocha, Carbon black-integrated polylactic acid 3D-printedsensors for the voltammetric determination of pyrogallic acid: Experimental and computational insights, Electrochim. Acta. 541 (2025). https://doi.org/10.1016/j.electacta.2025.147339.

[10] H.H. Bin Hamzah, O. Keattch, D. Covill, B.A. Patel, The effects of printing orientation on the electrochemical behaviour of 3D printed acrylonitrile butadiene styrene (ABS)/carbon black electrodes, Sci. Rep. 8 (2018) 1–8.

View Article Online
DOI: 10.1039/D6SD00005C

https://doi.org/10.1038/s41598-018-27188-5.

[11] T.T. Conrado, E.R. Pedão, V.S. Ferreira, K. Motta, A.C.A. Silva, R.A.B. da Silva, J.M. Petroni, B.G. Lucca, Sensitive, Integrated, Mass-produced, Portable and Low-cost Electrochemical 3D-printed Sensing Set (SIMPLE-3D-SenS): A promising analytical tool for forensic applications, Sensors Actuators B Chem. 427 (2025). https://doi.org/10.1016/j.snb.2024.137215.

[12] K. Dalvand, A. Ghiasvand, S. Keshan-Balavandy, F. Li, M. Breadmore, A simple 3D printed microfluidic device for point-of-care analysis of urinary uric acid, Aust. J. Chem. 76 (2023) 74–80. https://doi.org/10.1071/CH22180.

[13] V. Katic, P.L. Dos Santos, M.F. Dos Santos, B.M. Pires, H.C. Loureiro, A.P. Lima, J.C.M. Queiroz, R. Landers, R.A.A. Muñoz, J.A. Bonacin, 3D Printed Graphene Electrodes Modified with Prussian Blue: Emerging Electrochemical Sensing Platform for Peroxide Detection, ACS Appl. Mater. Interfaces. 11 (2019) 35068–35078. https://doi.org/10.1021/acsami.9b09305.

[14] Y. Kadri, I. Bekri-Abbess, P. Herrasti, Highly Sensitive Enzyme-free Sensor Based on a Carbon Paste Electrode Modified with Binary Zinc Oxide/Polyaniline Nanocomposites for Dopamine, Ascorbic Acid and Uric Acid Sensing, Electroanalysis. 35 (2023) 1–14. https://doi.org/10.1002/elan.202200248.

[15] N. Sittihakote, P. Danvirutai, S. Anutrakulchai, A. Tuantranont, C. Srichan, Empowering an Acute Kidney Injury 3D Graphene-Based Sensor Using Extreme Learning Machine, ACS Omega. 9 (2024) 21276–21286. https://doi.org/10.1021/acsomega.4c01315.

[16] C.L. Gonzalez-Gallardo, N. Arjona, L. Álvarez-Contreras, M. Guerra-Balcázar, Electrochemical creatinine detection for advanced point-of-care sensing devices: a review, RSC Adv. 12 (2022) 30785–30802. https://doi.org/10.1039/d2ra04479j.

[17] D.L. Glasco, A. Sheelam, N.H.B. Ho, J.G. Bell, Smartphone-based detection of levodopa in human sweat using 3D printed sensors, Anal. Chim. Acta. 1273 (2023) 341546. https://doi.org/10.1016/j.aca.2023.341546.

[18] R.M. Cardoso, D.M.H. Mendonça, W.P. Silva, M.N.T. Silva, E. Nossol, R.A.B. da Silva, E.M. Richter, R.A.A. Muñoz, 3D printing for electroanalysis: From multiuse electrochemical cells to sensors, Anal. Chim. Acta. 1033 (2018) 49–57. https://doi.org/https://doi.org/10.1016/j.aca.2018.06.021.

[19] A. Morais, D.P. Rocha, M.L. Felsner, A. Galli, Sustainable validated methodology for enzymeless determination of Tyrosine using 3D-printed PLA/CB electrodes in

View Article Online
DOI: 10.1039/D6SD00005C

synthetic urine, Talanta Open. 11 (2025) 100469. https://doi.org/10.1016/j.talo.2025.100469.

[20] M. Parrilla, N. Claes, C. Toyos-Rodríguez, C.E.M.K. Dricot, A. Steijlen, S. Lebeer, S. Bals, K. De Wael, Wearable 3D-printed solid microneedle voltammetric sensors based on nanostructured gold for uric acid monitoring, Biosens. Bioelectron. 289 (2025) 117934. https://doi.org/10.1016/j.bios.2025.117934.

[21] M.N. Islam, R.B. Channon, Electrochemical sensors, Bioeng. Innov. Solut. Cancer. (2019) 47–71. https://doi.org/10.1016/B978-0-12-813886-1.00004-8.

[22] F. Gao, C. Liu, L. Zhang, T. Liu, Z. Wang, Z. Song, H. Cai, Z. Fang, J. Chen, J. Wang, M. Han, J. Wang, K. Lin, R. Wang, M. Li, Q. Mei, X. Ma, S. Liang, G. Gou, N. Xue, Wearable and flexible electrochemical sensors for sweat analysis: a review, Microsystems Nanoeng. 9 (2023) 1–21. https://doi.org/10.1038/s41378-022-00443-6.

[23] Y.G. Park, S. Lee, J.U. Park, Recent progress in wireless sensors for wearable electronics, Sensors (Switzerland). 19 (2019) 1–34. https://doi.org/10.3390/s19204353.

[24] Y. Liu, Y. Dong, M. Hui, L. Xu, L. Ye, J. Lv, L. Yang, Y. Cui, A biosensing array for multiplex clinical evaluation of glucose, creatinine, and uric acid, Biosens. Bioelectron. 241 (2023) 115699. https://doi.org/https://doi.org/10.1016/j.bios.2023.115699.

[25] S.R.S. Pour, D. Calabria, A. Emamiamin, E. Lazzarini, A. Pace, M. Guardigli, M. Zangheri, M. Mirasoli, Microfluidic-Based Non-Invasive Wearable Biosensors for Real-Time Monitoring of Sweat Biomarkers, Biosensors. 14 (2024). https://doi.org/10.3390/bios14010029.

[26] A. Singh, A. Sharma, A. Ahmed, A.K. Sundramoorthy, H. Furukawa, S. Arya, A. Khosla, Recent advances in electrochemical biosensors: Applications, challenges, and future scope, Biosensors. 11 (2021) 1–31. https://doi.org/10.3390/bios11090336.

[27] R. Kale, M.K. Das, A.D. Gowda, S.A. Raut, J. Pannikkandathil, S. Bodake, R.M. Borkar, S. Pahal, S. Kumar, Direct Printing of an Electrochemical Device and Its Interface with Paper for Uric Acid Detection in Human Sweat, ACS Appl. Bio Mater. 8 (2025) 870–878. https://doi.org/10.1021/acsabm.4c01706.

[28] S. Meng, Y. Liu, L. Wang, X. Ji, Y. Chen, T. Zheng, J. Yu, H. Feng, Graphene-Based Flexible Sensors for Simultaneous Detection of Ascorbic Acid, Dopamine, and Uric Acid, Front. Bioeng. Biotechnol. 9 (2021) 1–12. https://doi.org/10.3389/fbioe.2021.726071.

[29] R.M. Cardoso, P.R.L. Silva, A.P. Lima, D.P. Rocha, T.C. Oliveira, T.M. do Prado, E.L. Fava, O. Fatibello-Filho, E.M. Richter, R.A.A. Muñoz, 3D-Printed graphene/polylactic acid electrode for bioanalysis: Biosensing of glucose and simultaneous determination of uric acid and nitrite in biological fluids, Sensors Actuators, B Chem. 307 (2020) 127621. https://doi.org/10.1016/j.snb.2019.127621.

[30] P. Dutta, V. Sharma, H. Bhardwaj, V.V. Agrawal, Rajesh, G. Sumana, Fabrication of Electrochemical Biosensor Using Zinc Oxide Nanoflowers for the Detection of Uric Acid, Mapan - J. Metrol. Soc. India. 37 (2022) 585–595. https://doi.org/10.1007/s12647-022-00598-7.

[31] S.S. Chaus, S. Lal, A. SP, P.G. Bahubalindruni, A flexible and highly sensitive non-enzymatic electrochemical sensing platform with readout electronics for sensing uric acid in human urine: Towards devices, Electrochim. Acta. 539 (2025) 147114. https://doi.org/10.1016/j.electacta.2025.147114.

[32] W. Yang, J. Fei, W. Xu, H. Jiang, M. Sakran, J. Hong, W. Zhu, X. Zhou, A biosensor based on the biomimetic oxidase Fe3O4@MnO2 for colorimetric determination of uric acid, Colloids Surfaces B Biointerfaces. 212 (2022) 112347. https://doi.org/10.1016/j.colsurfb.2022.112347.

[33] K. Fan, J. Zeng, C. Yang, G. Wang, K. Lian, X. Zhou, Y. Deng, G. Liu, Digital Quantification Method for Sensitive Point-of-Care Detection of Salivary Uric Acid Using Smartphone-Assisted μpADs, ACS Sensors. 7 (2022) 2049–2057. https://doi.org/10.1021/acssensors.2c00854.

[34] S.Y. Lee, D.S. Ciou, H.Y. Lee, J.Y. Chen, Y.C. Wei, M.D. Shieh, Portable Electrochemical System and Platform with Point-of-Care Determination of Urine Albumin-to-Creatinine Ratio to Evaluate Chronic Kidney Disease and Cardiorenal Syndrome, Biosensors. 14 (2024). https://doi.org/10.3390/bios14100463.

[35] D. Desai, A. Kumar, D. Bose, M. Datta, Ultrasensitive sensor for detection of early stage chronic kidney disease in human, Biosens. Bioelectron. 105 (2018) 90–94. https://doi.org/https://doi.org/10.1016/j.bios.2018.01.031.

[36] S. Fabre, P. Clerson, J.M. Launay, J.F. Gautier, T. Vidal-Trecan, J.P. Riveline, A. Platt, A. Abrahamsson, J.N. Miner, G. Hughes, P. Richette, T. Bardin, Accuracy of the HumaSens plus point-of-care uric acid meter using capillary blood obtained by fingertip puncture, Arthritis Res. Ther. 20 (2018) 1–9. https://doi.org/10.1186/s13075-018-1585-0.

[37] V.N. Ataide, D.P. Rocha, A. de Siervo, T.R.L.C. Paixão, R.A.A. Muñoz, L. Angnes,

Additively manufactured carbon/black-integrated polylactic acid 3Dprintedsensor for simultaneous quantification of uric acid and zinc in sweat, Microchim. Acta. 188 (2021) 1–11. https://doi.org/10.1007/s00604-021-05007-5.

[38] M.J.C. Matter, M. Rjeb, A. Labzour, A. Rjeb, S. Sayouri, M.C. El Idrissi, S. Massey, A. Adnot, D. Roy, C.M. Society, CONTRIBUTION TO THE STUDY BY X-RAY PHOTOELECTRON SPECTROSCOPY OF THE NATURAL AGING OF THE 2 . Experimental Procedure, 5 (2004) 1–5.

[39] M. Parrilla, N. Claes, C. Toyos-Rodríguez, C.E.M.K. Dricot, A. Steijlen, S. Lebeer, S. Bals, K. De Wael, Wearable 3D-printed solid microneedle voltammetric sensors based on nanostructured gold for uric acid monitoring, Biosens. Bioelectron. 289 (2025) 117934. https://doi.org/https://doi.org/10.1016/j.bios.2025.117934.

[40] E. Gaya, N. Menendez, E. Mazario, P. Herrasti, Fe3O4-Nanoparticle-Modified Sensor for the Detection of Dopamine, Uric Acid and Ascorbic Acid, Chemosensors. 11 (2023). https://doi.org/10.3390/chemosensors11020079.

[41] A.O. Alves, L. V. de Faria, N.M. Caldas, A.G. Batista, S.F.L. do Nascimento, B.E. Danho, D.A. Peixoto, E. Nossol, D.P. Rocha, F.S. Semaan, W.F. Pacheco, R.M. Dornellas, 3D-printed carbon black/polylactic acid electrode modified with silver particles: a powerful alternative and cost-effective sensor for nitrate sensing in real water samples, J. Solid State Electrochem. 29 (2025) 1217–1225. https://doi.org/10.1007/s10008-024-05919-1.

[42] S. Kumar, J.M. Mohan, K. Amreen, S.K. Dubey, S. Goel, A miniaturized unmodified toray paper-based electrochemical sensing platform for antipsychotic drug analysis, Sensors Actuators A Phys. 360 (2023) 114520. https://doi.org/10.1016/j.sna.2023.114520.

[43] S. Kumar, A.K. Bhagat, M. Bhaiyya, K. Amreen, S.K. Dubey, S. Goel, A Machine Learning Approach for Simultaneous Electrochemical Detection of Dopamine and Serotonin in an Optimized Carbon Thread-Based Miniaturized Device, IEEE Sens. J. 24 (2024) 21378–21385. https://doi.org/10.1109/JSEN.2024.3386655.

[44] J.M. Mohan, S. Kumar, K. Amreen, A. Javed, S.K. Dubey, S. Goel, Disposable Paper Based Miniaturized Device for Sensing of Phthalates, IEEE Sens. J. PP (2023) 1. https://doi.org/10.1109/JSEN.2023.3277797.

[45] Z. Xu, M. qi Zhang, H. qun Zou, J. shan Liu, D. zhi Wang, J. Wang, L. ding Wang, Non-enzymatic electrochemical detection of uric acid with electrodeposited Nafion film, J. Electroanal. Chem. 841 (2019) 129–134.

View Article Online
DOI: 10.1039/D6SD00005C

https://doi.org/10.1016/j.jelechem.2019.04.028.

[46] A.G. Cardoso, H. Viltres, G.A. Ortega, V. Phung, R. Grewal, H. Mozaffari, S.R. Ahmed, A.R. Rajabzadeh, S. Srinivasan, Electrochemical sensing of analytes in saliva: Challenges, progress, and perspectives, TrAC - Trends Anal. Chem. 160 (2023) 116965. https://doi.org/10.1016/j.trac.2023.116965.

[47] M. Yang, H. Wang, P. Liu, J. Cheng, A 3D electrochemical biosensor based on Super-Aligned Carbon NanoTube array for point-of-care uric acid monitoring, Biosens. Bioelectron. 179 (2021) 113082. https://doi.org/https://doi.org/10.1016/j.bios.2021.113082.

[48] P. Noppawan, J. Jakmunee, A.J. Hunt, N. Supanchaiyamat, S. Sangon, J. Lerdsri, T. Kruatian, J. Upan, Sustainable uric acid sensor based on a lab-fabricated electrode modified with rice straw-derived carbon materials, Sci. Rep. 15 (2025) 18380. https://doi.org/10.1038/s41598-025-03405-w.

[49] W. Liu, Y. Nie, M. Zhang, K. Yan, M. Wang, Y. Guo, Q. Ma, A novel nanosponge–hydrogel system-based electrochemiluminescence biosensor for uric acid detection, Luminescence. 37 (2022) 1524–1531. https://doi.org/https://doi.org/10.1002/bio.4326.

[50] S. Verma, J. Choudhary, K.P. Singh, P. Chandra, S.P. Singh, Uricase grafted nanoconducting matrix based electrochemical biosensor for ultrafast uric acid detection in human serum samples, Int. J. Biol. Macromol. 130 (2019) 333–341. https://doi.org/10.1016/j.ijbiomac.2019.02.121.

View Article Online
DOI: 10.1039/D6SD00005C

The data supporting this article have been included in the main article and / or as part of the Supplementary Information.